

[ATLAS Semivisible Jets]

[Elena Laura Busch]

Submitted in partial fulfillment of the
requirements for the degree of
Doctor of Philosophy
under the Executive Committee
of the Graduate School of Arts and Sciences

COLUMBIA UNIVERSITY

2023

© 2023

[Elena Laura Busch]

All Rights Reserved

Abstract

[ATLAS Semivisible Jets]

[Elena Laura Busch]

[illegible]

[illegible]

conclusions reached. Individual chapters should not have abstracts.

Table of Contents

List of Figures

List of Tables

Acknowledgements

Insert your acknowledgements text here. This page is optional, you may delete it if not needed.

Dedication

Dedicated to my friends and family

Introduction or Preface

Insert your preface text here if applicable. This page is optional, you may delete it if not needed. If you delete this page make sure to move page counter comment in thesis.tex to correct location.

Chapter 1: The Standard Model

Four fundamental forces

The Standard Model is a universally accepted framework which explains most of the interactions of fundamental particles. The SM is a renormalizable quantum field theory that obeys the local symmetry G_{SM} :

$$G_{SM} = SU(3)_C \times SU(2)_L \times U(1)_Y \quad (1.1)$$

The $SU(3)_C$ symmetry component is the non-Abelian gauge group of quantum chromodynamics (QCD), which describe the physics of strongly interacting particles. There are 8 generators for the $SU_C(3)$ group which correspond to *gluons*, massless spin-1 gauge boson which carry the force of the strong interaction. Gluon and quarks, the particles which interact with the strong force, carry a color charge C .

The $SU(2)_L \times U(1)_Y$ symmetry group represents the electroweak sector of the SM. There are 4 generators for this group, which correspond to the four massless gauge bosons W^1 , W^2 , W^3 , and B . From these massless gauge bosons are formed the massive mediators of the weak force, the W^- , W^+ and Z^0 bosons, and the massless electromagnetic force carrier, the photon γ .

The interplay between the fermionic and bosonic fields that emerge from the G_{SM} symmetry can be described through the Lagrangian in equation ??

$$\mathcal{L} = \mathcal{L}_{kin} + \mathcal{L}_{\psi} + \mathcal{L}_{Yuk} + \mathcal{L}_{\phi} \quad (1.2)$$

Each term in this Lagrangian describes a set of specific particle physics interactions. \mathcal{L}_{kin} . with three families of quarks and leptons, and a scalar Higgs doublet. The standard model has 12 gauge bosons: 8 gluons, 3 weak bosons, and the photon. [pdg]

The physics of the Standard Model of particle physics (SM) is summarized by the SM La-

grangian:

$$\mathcal{L}_{kin} = -\frac{1}{4}F_{\mu\nu}F^{\mu\nu} \quad (1.3)$$

Explain equation

Explain phenomonolyg

Chapter 2: The Large Hadron Collider

The Large Hadron Collider (LHC) [**LHC_machine**] is a 26.7km long circular superconducting high-energy particle accelerator, located approximately 100m underground near the city of Geneva, Switzerland. The LHC occupies the tunnel constructed between 1984 and 1989 for the Large Electron-Positron Collider. It also borrows some injection infrastructure from the LEP machine. The LHC is operated by the European Organization for Nuclear Research (CERN), the largest international scientific collaboration in the world.

The LHC accelerates protons and heavy ions and collides them at four interaction points around the ring, with a design center-of-mass energy per collision of $\sqrt{s} = 14$ TeV. Each interaction point is home to one of four detector experiments, which study the products of the collisions. The largest of these experiments is the ATLAS detector [**ATLAS_at_LHC**], a general purpose detector for studying the Standard Model and searching for physics beyond it. The CMS detector [**CMS_at_LHC**] is another general purpose detector, designed and operated independently of the ATLAS detector, but intended to probe the same range of physics. The ALICE [**ALICE_at_LHC**] experiment is a dedicated heavy ion experiment, and the LHC-b [**LHCb_at_LHC**] experiment is a dedicated *b*-physics experiment.

The first proton-proton collisions at the LHC were achieved in 2010 at a center-of-mass energy of $\sqrt{s} = 7$ TeV. Run 1 of the LHC took place between 2010 and 2013. The data collected during this time led to the announcement of the discovery of the Higgs boson in 2012 [**higgs_paper**]. Between 2013 and 2015 the LHC underwent the first Long Shutdown (LS1) during which time key upgrades to the physics detectors and the accelerator chain were installed. Run 2 of the LHC was active from 2015 to 2018 and achieved a center-of-mass energy of $\sqrt{s} = 13$ TeV. Between 2018 and

2022 the LHC underwent the second Long Shutdown (LS2). Run-3 of the LHC began in 2022 and achieved a center-of-mass energy of $\sqrt{s} = 13.6$ TeV.

2.1 Accelerator Physics

2.1.1 The Journey of a Proton

Protons which feed the LHC start as hydrogen gas. The electrons are removed from the hydrogen atoms through the use of strong electric fields. The linear accelerator (LINAC) then accelerates the H^+ ions to an energy of 50 MeV. From here the H^+ ions enter the Proton Synchrotron booster, where they are accelerated up to 1.4 GeV of energy. Subsequently they are sorted into bunches separated in time by 25 ns, where each bunch contains approximately 10^{11} protons. Next the bunches pass through the Proton Synchrotron (PS) and the Super Proton Synchrotron (SPS), where they reach energies of 25 GeV and 450 GeV respectively. Finally they are injected into the LHC as two beams traveling in opposite direction, and can be accelerated up to 7 TeV of energy. Due to limitations with the magnet training, the highest energy actually achieved by the LHC beams during Run 2 was 6.5 TeV each, giving a collision center-of-mass energy of $\sqrt{s} = 13$ TeV. Figure ?? shows the full LHC accelerator complex.

Acceleration in the LHC is performed by eight radio frequency (RF) cavities located around the ring. Each RF cavity produces a 2MV electric field oscillating at 40 MHz. This oscillation is synchronized with the occurrence of the proton bunches produced in the PS. The 40MHz oscillation produces points of stable equilibrium every 2.5ns – a proton bunch occupies this point of stable equilibrium one out of every ten times, such that the bunches maintain their 25ns spacing. This is illustrated in figure ??.

In addition to the acceleration cavities, the LHC houses 9593 superconducting electromagnets which direct and focus the proton beam on its 27km journey. The magnets are comprised of superconducting Niobium-Titanium coils cooled by superfluid helium at 1.4 K. As the beams approach

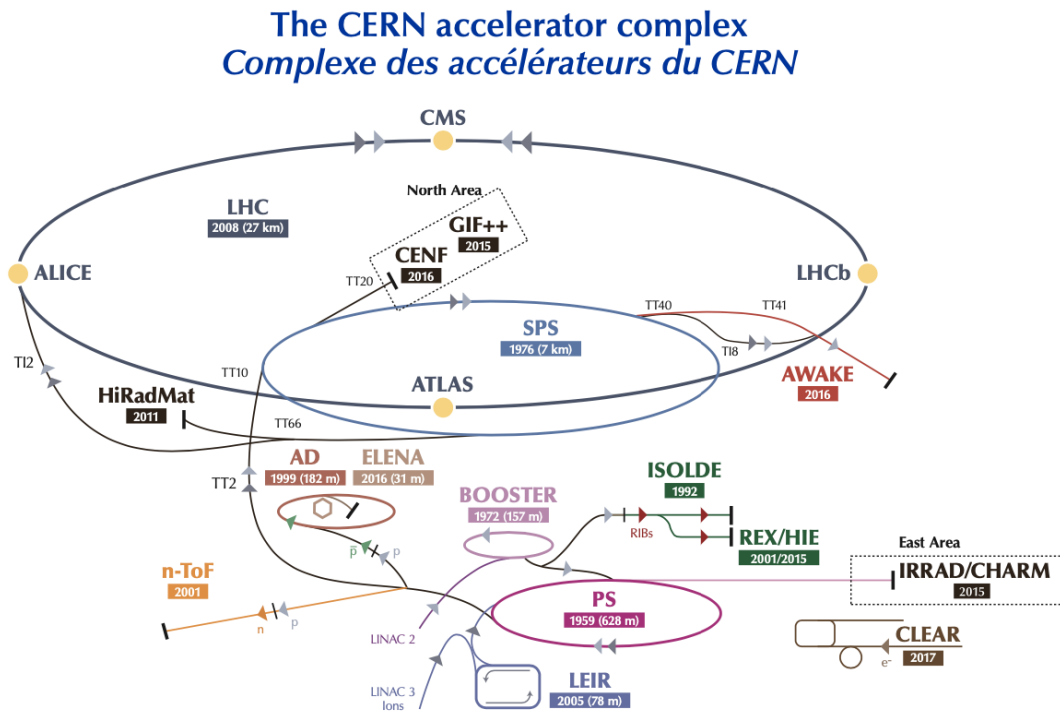


Figure 2.1: The LHC accelerator complex at CERN [cern_accelerator_complex]

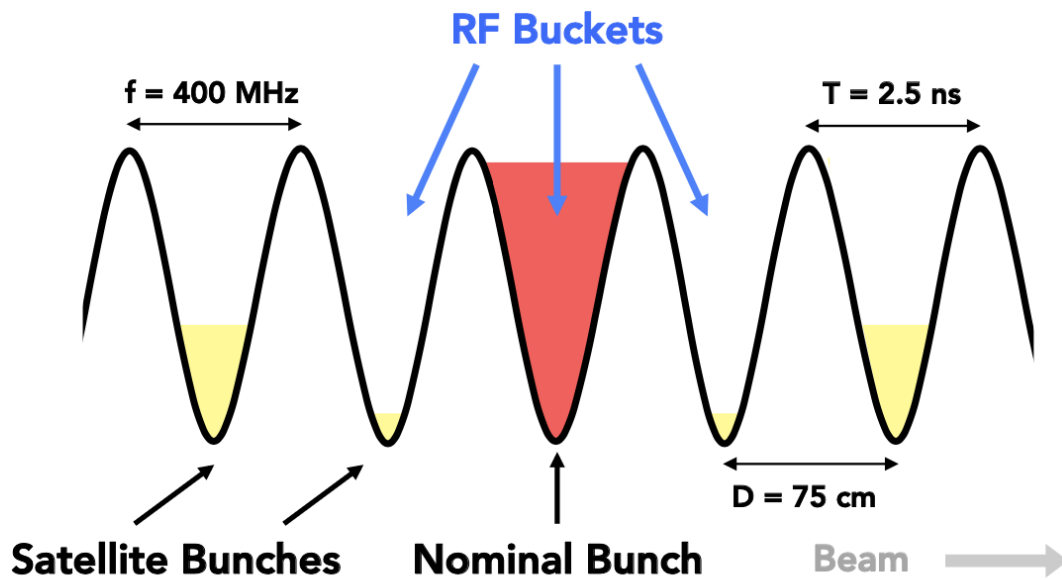


Figure 2.2: The LHC accelerator complex at CERN

one of the four collision points around the ring, additional multipole magnets focus and squeeze the beam for optimal collisions.

2.1.2 Luminosity

Collisions at the LHC occur when the two beams of proton bunches cross at one of the four interaction points. The intensity of collisions is described by the instantaneous luminosity, the formula for which is given in equation ?? The instantaneous luminosity gives the number of the collisions that could be produced at the interaction point per cm^2 of cross-sectional area per second. The integrated luminosity is obtained by integrating the instantaneous luminosity over time, and measures the total number of collisions which has occurred over the course of running. This is directly correlated with the size of the datasets collected by the LHC experiments.

$$= \frac{N_1 N_2}{4\pi\sigma_x\sigma_y} \quad (2.1)$$

The design peak luminosity of the LHC is $1.0 \times 10^{34} cm^{-2}s^{-1}$. During Run 1 of the LHC the peak instantaneous luminosity achieved was $0.8 \times 10^{34} cm^{-2}s^{-1}$. Over the course of Run 1 the LHC collected a total integrated luminosity of $5.46 fb^{-1}$ at $\sqrt{s} = 7TeV$, and $22.8 fb^{-1}$ at $\sqrt{s} = 8TeV$. Following the first long shutdown and upgrade phase of operations, the LHC achieved a center of mass energy $\sqrt{s} = 13TeV$ at the beginning of Run 2 in 2015. The LHC was also able to deliver $2.0 \times 10^{34} cm^{-2}s^{-1}$ peak instantaneous luminosity, double the design value. During LHC Run 2, from 2015-2018, the LHC delivered $= 156 fb^{-1}$ of integrated luminosity for proton-proton collisions. Run 3 of the LHC began in 2022, and is expected to deliver $250 fb^{-1}$ of integrated luminosity to the ATLAS and CMS experiments by 2026.

Chapter 3: The ATLAS Detector

The ATLAS detector is one of two general purpose physics detectors designed to study the products of the proton-proton collisions produced by the LHC. The detector is composed of a variety of specialized subsystems, designed to fully capture the large array of physics processes produced in the LHC. The apparatus is 25m high, 44m in length, and weighs over 7000 tons. Collisions occur directly in the center of the apparatus, and the cylindrical design of the detector allows a complete 360 view of any physics objects resulting from the collision to be reconstructed.

Two magnet systems provide strong magnetic fields, which bend the trajectory of charged particles as they pass through the magnetic fields; this allows the calculation of the momentum of the particles. A 2T solenoid magnet provides a uniform magnetic field to the inner layers of the detector. Further out, a toroidal magnet system (TODO: how many toroids?) provides fields strengths of 0.5 to 1T

3.1 Coordinate System and Geometry

The ATLAS detector employs a right hand cylindrical coordinate system. The z axis is aligned with the beam line, and the x - y plane sits perpendicular to the beam line. The origin is centered on the detector, such that the origin corresponds with the interaction point of the two colliding beams. The detector geometry is usually characterized by polar coordinates, where the azimuthal angle ϕ spans the x - y plane. The polar angle θ represents the angle away from the beam line, or z axis. $\theta = 0$ aligns with the positive z -axis, and $\phi = 0$ aligns with the positive x -axis.

The polar coordinate θ is generally replaced by the Lorentz invariant quantity *rapidity*.

$$y = \frac{1}{2} \ln\left(\frac{E + p_z}{E - p_z}\right) \quad (3.1)$$

This substitution is advantageous because objects in the detector are traveling at highly relativistic speeds. The relativistic speed of objects passing through the ATLAS detector also means that the masses of the particles are generally small compared to their total energy. In the limit of zero mass, the rapidity y reduces to the *pseudorapidity* η , which can be calculated directly from the polar angle θ .

$$\eta = -\ln\left(\frac{\theta}{2}\right) \quad (3.2)$$

Figure ?? depicts the orientation of the coordinate system with respect to the ATLAS detector, while Figure ?? illustrates the relationship between θ , η , and the beamline axis z . The distance between physics objects in the detector is generally expressed in terms of the solid angle between them ΔR .

$$\Delta R = \sqrt{\Delta\phi^2 + \Delta\eta^2} \quad (3.3)$$

Head on proton-proton collisions are more likely to result in objects with a lot of energy in the transverse plane; glancing proton-proton collisions are more likely to result in objects where most of the energy is directed along the z -axis. Due to the importance of categorizing these objects, as well as the cylindrical design of the ATLAS detector, the detector is generally divided into regions in η . Each subsystem has a “central” or “barrel” region covering low $|\eta|$, while the “forward” or “endcap” regions cover $|\eta|$ up to 4.9. Each of the three main ATLAS subsystems will be discussed in the following sections.

TODO: include figures (subfigure)

3.2 Inner Detector

The Inner Detector (ID) is the ATLAS subsystem closest to the interaction point. The primary purpose of the ID is to determine the charge, momentum, and trajectory of charged particles passing through the detector. With this information the ID is also able to precisely determine interaction vertices.

The ID is composed of three sub-detectors; the pixel detector, the semiconductor tracker (SCT) and the transition radiation tracker (TRT). Figure ?? shows the location of these three subsystems with respect to each other and the interaction point.

3.2.1 Pixel Detector

The pixel detector is the first detector encountered by particles produced in LHC collisions. The original pixel detector consists of 3 barrel layers of silicon pixels, positioned at 4cm, 11cm and 14cm from the beamline. There are also 4 disks on each side positioned between 11 and 20cm, providing full coverage $|\eta| < 2.5$. The layers are comprised of silicon pixels each measuring $50\ \mu\text{m}$ by $300\ \mu\text{m}$, with 140 million pixels in total. The pixels are organized into modules, which each contain a set of radiation hard readout electronics chips. In 2014, the Insertable B-layer (IBL) was installed, creating a new innermost layer of the pixel detector sitting just 3.3cm from the beamline. The pixels of the IBL measure $50\ \mu\text{m}$ by $250\ \mu\text{m}$, and cover a pseudo-rapidity range up to $|\eta| < 3$. The IBL upgrade enhances the pixel detector's ability to reconstruct secondary vertices associated with short-lived particles such as the b-quark. The improved vertex identification also helped compensate for increasing pile-up in Run 2.

3.2.2 Semiconductor Tracker

The SCT provides at least 4 additional measurements of each charged particle. It employs the same silicon technology as the Pixel Detector, but utilizes larger silicon strips which measure

$80\mu\text{m}$ by 12.4cm . The SCT is composed of 4 barrel layers, located between 30cm and 52cm from the beamline, and 9 end-cap layers on each side. The SCT can distinguish tracks that are separated by at least $200\mu\text{m}$.

3.2.3 Transition Radiation Tracker

The TRT provides an additional 36 hits per particle track. The detector relies on gas filled straw tubes, a technology which is intrinsically radiation hard. The straws which are each 4mm in diameter and up to 150cm in length and filled with xenon gas. The detector is composed of about 50000 barrel region straws and 640000 end-cap straws, comprising 420000 electronic readout channels. Each channel provides a drift time measurement with a spatial resolution of $170\mu\text{m}$ per straw. As charged particles pass through the detector and interact with the xenon, transition radiation is emitted. The use of two different drift time thresholds allows the detector to distinguish between tracking hits and transition radiation hits.

3.3 Calorimeters

The ATLAS calorimeter system is responsible for measuring the energy of electromagnetically and hadronically interacting particles passing through the detector. The calorimeters are located just outside the central solenoid magnet, which encloses the inner detectors. The ATLAS calorimetry system is composed of two subsystems - the Liquid Argon (LAr) calorimeter for electromagnetic calorimetry and the Tile calorimeter for hadronic calorimetry. The full calorimetry system is showing in figure ??.

3.4 Liquid Argon Calorimeter

The LAr calorimeter is specifically designed to measure the energies of electromagnetic EM particles such as electrons and photons.

Conclusion or Epilogue

[illegible]

[illegible]

[illegible]

Otherwise, you may delete it. Use this page for your epilogue or conclusion if applicable; please
use only one of the titles for this page. Otherwise, you may delete it. Use this page for your
epilogue or conclusion if applicable; please use only one of the titles for this page. Otherwise,
you may delete it. Use this page for your epilogue or conclusion if applicable; please use only one
of the titles for this page. Otherwise, you may delete it. Use this page for your epilogue or
conclusion if applicable; please use only one of the titles for this page. Otherwise, you may delete
it. Use this page for your epilogue or conclusion if applicable; please use only one of the titles for
this page. Otherwise, you may delete it. Use this page for your epilogue or conclusion if
applicable; please use only one of the titles for this page. Otherwise, you may delete it. Use this
page for your epilogue or conclusion if applicable; please use only one of the titles for this page.
Otherwise, you may delete it. Use this page for your epilogue or conclusion if applicable; please
use only one of the titles for this page. Otherwise, you may delete it. Use this page for your
epilogue or conclusion if applicable; please use only one of the titles for this page. Otherwise,
you may delete it. Use this page for your epilogue or conclusion if applicable; please use only one
of the titles for this page. Otherwise, you may delete it. Use this page for your epilogue or
conclusion if applicable; please use only one of the titles for this page. Otherwise, you may delete
it.

Appendix A: Experimental Equipment

Lorem ipsum dolor sit amet, consectetur adipiscing elit, sed do eiusmod tempor incididunt ut labore et dolore magna aliqua. Ut enim ad minim veniam, quis nostrud exercitation ullamco laboris nisi ut aliquip ex ea commodo consequat. Duis aute irure dolor in reprehenderit in voluptate velit esse cillum dolore eu fugiat nulla pariatur. Excepteur sint occaecat cupidatat non proident, sunt in culpa qui officia deserunt mollit anim id est laborum.

Appendix B: Data Processing

Lorem ipsum dolor sit amet, consectetur adipiscing elit, sed do eiusmod tempor incididunt ut labore et dolore magna aliqua. Ut enim ad minim veniam, quis nostrud exercitation ullamco laboris nisi ut aliquip ex ea commodo consequat. Duis aute irure dolor in reprehenderit in voluptate velit esse cillum dolore eu fugiat nulla pariatur. Excepteur sint occaecat cupidatat non proident, sunt in culpa qui officia deserunt mollit anim id est laborum.